Theory of tracer diffusion in concentrated hard-sphere suspensions

S. S. L. Peppin

A phenomenological theory of diffusion and cross-diffusion of tracer particles in concentrated hard-sphere suspensions is developed within the context of Batchelor's theory of multicomponent diffusion. Expressions for the diffusion coefficients as functions of the host particle volume fraction are obtained up to the close-packing limit. In concentrated systems the tracer diffusivity decreases because of the reduced pore space available for diffusion. Tracer diffusion, and segregation during sedimentation, ceases at a critical trapping volume fraction. The tracer diffusivity can be modelled by a Stokes-Einstein equation with an effective viscosity that depends on the pore size. The tracer cross-diffusion coefficient increases near the glass transition and diverges in the close-packed limit.

Key words: colloidal suspensions, diffusion, sedimentation

1. Introduction

In contrast to normal Brownian diffusion in liquids, tracer diffusion in complex systems such as colloidal suspensions is strongly hindered and anomalous (Wang *et al.* 2012; Metzler *et al.* 2014). Modelling such systems is challenging owing to competing nonlinear effects, including long-range viscous interactions between the tracer particles and host matrix. In this work some progress is made in the case of a hard-sphere suspension containing spherical tracer particles in the pore fluid. Batchelor (1976, 1983, 1986) solved the hydrodynamic equations describing this system in the dilute limit and obtained expressions for the diffusion coefficients to first order in the particle volume fractions. Later researchers obtained similar results starting from the Smoluchowski and Fokker-Planck equations (Zhang & Nagele 2002; Bruna & Chapman 2012) or by using thermodynamic methods (Vergara *et al.* 2001; Annunziata 2008), while recent efforts have employed Stokesian and molecular dynamics simulations (Wang & Brady 2015; Hannam *et al.* 2017). In many 'crowded' systems the host particles are at non-dilute volume fractions near to and above the glass transition, where long-range viscous effects and nonlinear particle-particle interactions are predominant (Wang *et al.* 2012; Guan *et al.* 2014; Sentjabrskaja1 *et al.* 2016). In order to obtain expressions for the diffusion coefficients at these high concentrations, here a phenomenological approach is used, in which nonequilibrium thermodynamics is combined with capillary flow models and empirical data.

In Section 2 the irreversible thermodynamics equations describing cross diffusion are described, and Batchelor's theory of multicomponent diffusion is briefly reviewed. In Section 3 the equations are written in a membrane transport framework in order to obtain expressions for the diffusion coefficients in terms of experimentally convenient quantities such as the permeability and osmotic pressure. Expressions for these quantities are combined in Section 4 with Batchelor's results to obtain the diffusion coefficients

as functions of the host particle volume fraction. Section 5 presents some results and comparison with experiment; Section 6 contains a discussion of sedimentation, the Stokes-Einstein equation, and the physical interpretation and measurement of parameters.

2. Diffusion and cross-diffusion in hard-sphere suspensions

2.1. *Flux equations*

From irreversible thermodynamics (deGroot & Mazur 1962; Batchelor 1986) the diffusion fluxes in a binary hard-sphere suspension can be written as

$$\boldsymbol{J}_1 = -L_{11}\boldsymbol{\nabla}\mu_1 - L_{12}\boldsymbol{\nabla}\mu_2, \qquad (2.1a)$$

$$\boldsymbol{J}_2 = -L_{21}\boldsymbol{\nabla}\mu_1 - L_{22}\boldsymbol{\nabla}\mu_2, \qquad (2.1b)$$

where the L_{ij} are phenomenological coefficients, $\boldsymbol{J}_i = n_i(\boldsymbol{u}_i - \boldsymbol{u})$ is the flux of i moving at average velocity $\boldsymbol{u}_i$ relative to the volume-average velocity $\boldsymbol{u}$ of the mixture, and n_i is the concentration of i (number of particles per unit volume of mixture). If the system is not too far from equilibrium, the L_{ij} obey the Onsager relation (deGroot & Mazur 1962; Batchelor 1986)

$$L_{12} = L_{21}. \qquad (2.2)$$

In (2.1) $\mu_i = \mu_i^a - v_i\mu_0^a/v_0$ are effective (reduced) chemical potentials, where μ_i^a is the actual chemical potential per particle of component i (0 is the fluid, assumed incompressible, 1 is the host particles and 2 is the tracer particles), and $v_i = \frac{4}{3}\pi R_i^3$ is the volume of a particle of radius R_i. When the suspending fluid is incompressible and composed of molecules that are much smaller than the hard-sphere particles, the reduced chemical potentials in a hard-sphere suspension are equivalent to the chemical potentials of a hard-sphere gas at the same volume fractions (Russel *et al.* 1989; Batchelor 1983; Annunziata 2008).

At constant mixture pressure P and temperature T the chemical potentials depend on the concentrations n_1 and n_2, so that

$$\boldsymbol{\nabla}\mu_1 = \mu_{11}\boldsymbol{\nabla}n_1 + \mu_{12}\boldsymbol{\nabla}n_2, \qquad (2.3a)$$

$$\boldsymbol{\nabla}\mu_2 = \mu_{21}\boldsymbol{\nabla}n_1 + \mu_{22}\boldsymbol{\nabla}n_2,, \qquad (2.3b)$$

where $\mu_{ij} = (\partial\mu_i/\partial n_j)_{T,P,n_{k\neq j}}$. Equations (2.1) can then be written as

$$\boldsymbol{J}_1 = -D_{11}\boldsymbol{\nabla}n_1 - D_{12}\boldsymbol{\nabla}n_2, \qquad (2.4a)$$

$$\boldsymbol{J}_2 = -D_{21}\boldsymbol{\nabla}n_1 - D_{22}\boldsymbol{\nabla}n_2, \qquad (2.4b)$$

where the diffusion coefficients D_{ij} are

$$D_{11} = L_{11}\mu_{11} + L_{12}\mu_{21}, \qquad D_{12} = L_{11}\mu_{12} + L_{12}\mu_{22}, \qquad (2.5a,b)$$

$$D_{21} = L_{21}\mu_{11} + L_{22}\mu_{21}, \qquad D_{22} = L_{21}\mu_{12} + L_{22}\mu_{22}. \qquad (2.5c,d)$$

Here D_{11} is the main Fickian diffusion coefficient of the host particles, while D_{12} is a cross-diffusion coefficient characterizing motion of the host particles caused by a gradient in tracer particle concentration $\boldsymbol{\nabla}n_2$. Similarly, D_{22} is the Fickian tracer diffusivity, while D_{21} accounts for motion of the tracer particles caused by a gradient in n_1.

2.2. *Batchelor's theory*

By calculating the bulk mobilities of spherical particles in a polydisperse suspension, Batchelor (1983, 1986) derived expressions for the phenomenological coefficients L_{ij} to

first order in the volume fractions $\phi_i = v_i n_i$. For a bidisperse suspension in the dilute tracer limit ($\phi_2 \ll \phi_1 \ll 1$) the L_{ij} are

$$L_{11} = \frac{n_1}{6\pi\eta_0 R_1}\left(1 + (K_{11}^{'} + K_{11}^{''})\phi_1\right), \qquad L_{12} = \frac{n_1}{6\pi\eta_0 R_1}\left(\lambda_{12}^{-3}K_{12}^{''}\phi_2\right), \quad (2.6a,b)$$

$$L_{21} = \frac{n_2}{6\pi\eta_0 R_2}\left(\lambda_{21}^{-3}K_{21}^{''}\phi_1\right), \qquad\qquad L_{22} = \frac{n_2}{6\pi\eta_0 R_2}\left(1 + K_{21}^{'}\phi_1\right), (2.6c,d)$$

where η_0 is the viscosity of the suspending fluid, $\lambda_{ij} = R_j/R_i$, $K_{ij}^{'} = -2.5/(1 + .22\lambda_{ij})$, and $K_{ij}^{''} = \lambda_{ij}^2/(1 + \lambda_{ij}^3) - (\lambda_{ij}^2 + 3\lambda_{ij} + 1) = \lambda_{ij}^2 K_{ji}^{''}$.

In the dilute limit the binary hard-sphere gas chemical potentials are

$$\mu_1 = \mu_1^0 + k_B T(\ln\phi_1 + b_{11}\phi_1 + b_{21}\phi_2), \tag{2.7a}$$

$$\mu_2 = \mu_2^0 + k_B T(\ln\phi_2 + b_{22}\phi_2 + b_{12}\phi_1), \tag{2.7b}$$

where k_B is Boltzmann's constant, μ_i^0 are constants (at constant T, P) and $b_{ij} = (1+\lambda_{ij})^3$ (Annunziata 2008; Santos & Rohrmann 2013). Differentiating (2.7) with respect to n_i gives

$$\mu_{11} = k_B T(n_1^{-1} + v_1 b_{11}), \qquad \mu_{12} = k_B T v_2 b_{21}, \tag{2.8a,b}$$

$$\mu_{21} = k_B T v_1 b_{12}, \qquad\qquad \mu_{22} = k_B T(n_2^{-1} + v_2 b_{22}). \tag{2.8c,d}$$

Combining (2.8) and (2.6) with (2.5) leads to Batchelor's expressions for the diffusion coefficients, in the limit $\phi_2 \ll \phi_1 \ll 1$, as

$$D_{11} = D_1^0(1 + 1.45\phi_1), \qquad D_{12} = D_1^0(b_{12} + K_{12}^{''})\phi_1, \tag{2.9a,b}$$

$$D_{21} = D_2^0(b_{21} + K_{21}^{''})\phi_2, \qquad D_{22} = D_2^0(1 + K_{21}^{'}\phi_1), \tag{2.9c,d}$$

where $D_i^0 = k_B T/6\pi\eta_0 R_i$ is the Stokes-Einstein diffusivity of component i.

3. Membrane transport formulation

Extending Batchelor's theory to higher volume fractions of the host particles is challenging because of the difficulty of determining higher-order expressions for the phenomenological coefficients. However, progress can be made by rewriting the L_{ij} and μ_{ij} in terms of the host-matrix permeability and osmotic pressure, for which experimental data and theoretical expressions are available.

3.1. *Osmotic equilibrium*

The chemical potentials can be replaced with osmotic pressures by considering the osmotic equilibrium system illustrated in figure 1. The suspension in compartment A at pressure P is in equilibrium across a semi-permeable partition with a reservoir at pressure p (compartment B) containing only the fluid and tracer particles. Compartment B is in turn in equilibrium with another reservoir (compartment C) that contains only the suspending fluid at pressure p_w. At equilibrium the tracer chemical potential μ_2 in the suspension is equal to the chemical potential μ_2^r of the tracer particles in the reservoir, so that

$$\mu_2 = \mu_2^r. \tag{3.1}$$

The Gibbs-Duhem equation applied to the suspension in A is, at constant T,

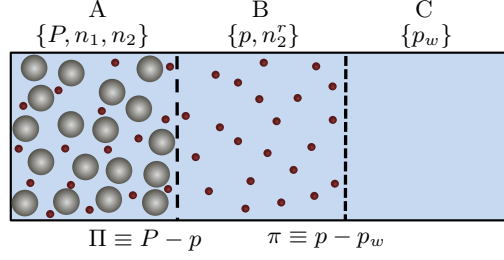$$n_1 d\mu_1 + n_2 d\mu_2 = d\Pi_T, \tag{3.2}$$

FIGURE 1. Illustration of osmotic equilibrium in a bidisperse hard-sphere suspension. P is the total mixture pressure of the suspension in compartment A; p is the pressure of the tracer suspension in B; and p_w is the pressure of the pure fluid in C. The membrane separating compartments A and B is permeable to the fluid (blue) and tracer particles (red) but impermeable to the larger host particles (grey). The difference between the pressures in A and B is the host particle osmotic pressure $\Pi \equiv P - p$. The membrane separating compartments B and C is permeable to the fluid but impermeable to the tracer particles; the tracer osmotic pressure is $\pi \equiv p - p_w$. Because of the volume taken up by the host particles, the tracer concentration n_2 in compartment A is less than the concentration n_2^r in the reservoir compartment B; $\alpha = n_2/n_2^r$ is the equilibrium partition coefficient.

where $\Pi_T \equiv P - p_w$ is the total osmotic pressure of the suspension. Equation (3.2) is a consequence of the analogy between hard-sphere fluids and hard-sphere suspensions, for which Π_T plays the role of pressure (Batchelor 1983; Russel *et al.* 1989; Annunziata 2008). The Gibbs-Duhem equation applied to the reservoir compartment B is

$$n_2^r \mathrm{d}\mu_2^r = \mathrm{d}\pi, \tag{3.3}$$

where $\pi \equiv p - p_w$ is the tracer osmotic pressure. Combining (3.1)–(3.3) gives

$$n_1 \mathrm{d}\mu_1 = \mathrm{d}\Pi + (1 - \alpha)\mathrm{d}\pi \qquad \text{and} \qquad n_2 \mathrm{d}\mu_2 = \alpha \mathrm{d}\pi, \tag{3.4a,b}$$

where $\alpha \equiv n_2/n_2^r$ is the equilibrium partition coefficient and $\Pi \equiv P - p$ is the host particle osmotic pressure. With the local equilibrium assumption (deGroot & Mazur 1962), equation (3.4) can be written in terms of gradients as

$$n_1 \boldsymbol{\nabla}\mu_1 = \boldsymbol{\nabla}\Pi + (1 - \alpha)\boldsymbol{\nabla}\pi \qquad \text{and} \qquad n_2 \boldsymbol{\nabla}\mu_2 = \alpha \boldsymbol{\nabla}\pi. \tag{3.5a,b}$$

Differentiating with respect to n_i gives

$$\mu_{11} = n_1^{-1}\left(\Pi_1 + (1 - \alpha)\pi_1\right), \qquad \mu_{12} = n_1^{-1}\left(\Pi_2 + (1 - \alpha)\pi_2\right), \tag{3.6a,b}$$
$$\mu_{21} = n_2^{-1}\alpha\pi_1, \qquad\qquad\qquad \mu_{22} = n_2^{-1}\alpha\pi_2, \tag{3.6c,d}$$

where $\Pi_i = (\partial\Pi/\partial n_i)_{T,P,n_{j\neq i}}$ and $\pi_i = (\partial\pi/\partial n_i)_{T,P,n_{j\neq i}}$.

3.2. *Membrane transport equations*

The phenomenological coefficients L_{ij} in (2.1) can be replaced with membrane transport quantities such as the host matrix permeability k by making a change of independent variables from $\{n_1, n_2\}$ to the reservoir parameters $\{p, n_2^r\}$. Assuming P is constant and that π depends only on n_2^r (isothermal incompressible fluid),

$$\boldsymbol{\nabla}\Pi = -\boldsymbol{\nabla}p \qquad \text{and} \qquad \boldsymbol{\nabla}\pi = \pi_r \boldsymbol{\nabla}n_2^r, \tag{3.7a,b}$$

where $\pi_r = (\partial\pi/\partial n_2^r)_{T,p}$. Inserting (3.7), (3.5) and (2.2) into (2.1) and rearranging leads to a hard-sphere suspension version of the membrane transport equations (Spiegler &

Kedem 1966),

$$\boldsymbol{q} = -\frac{k}{\eta_0} \left(\boldsymbol{\nabla} p - \sigma \boldsymbol{\nabla} \pi \right), \qquad (3.8a)$$

$$\boldsymbol{J} = n_2^r (1 - \sigma)\boldsymbol{q} - \alpha D_t \boldsymbol{\nabla} n_2^r, \qquad (3.8b)$$

where $\boldsymbol{q} = -\boldsymbol{J}_1/n_1 = \boldsymbol{u} - \boldsymbol{u}_1$ is the volume flux relative to the host particles and $\boldsymbol{J} = \boldsymbol{J}_2 - n_2 \boldsymbol{J}_1/n_1 = \alpha n_2^r (\boldsymbol{u}_2 - \boldsymbol{u}_1)$ is the tracer diffusive flux. The host matrix permeability k, reflection coefficient σ and tracer diffusivity D_t are defined by the equations

$$\frac{k}{\eta_0} \equiv -\left(\frac{\boldsymbol{q}}{\boldsymbol{\nabla} p} \right)_{\boldsymbol{\nabla}\pi=0}, \quad \sigma \equiv \left(\frac{\boldsymbol{\nabla} p}{\boldsymbol{\nabla} \pi} \right)_{\boldsymbol{q}=0}, \quad D_t \equiv -\left(\frac{\boldsymbol{J}/\alpha}{\boldsymbol{\nabla} n_2^r} \right)_{\boldsymbol{q}=0}, \quad (3.9a,b,c)$$

or, in terms of the phenomenological coefficients L_{ij},

$$\frac{k}{\eta_0} = \frac{L_{11}}{n_1^2}, \quad \sigma = 1 - \alpha \left(1 - \frac{L_{12} n_1}{L_{11} n_2} \right), \quad D_t = \frac{\pi_r}{n_2} \left(L_{22} - \frac{L_{12}^2}{L_{11}} \right). \quad (3.10a,b,c)$$

3.3. *Diffusion coefficients*

Inserting (3.10), (3.6) and (2.2) into (2.5) leads to

$$D_{11} = n_1 \frac{k}{\eta_0} \left(\Pi_1 + \sigma \pi_1 \right), \qquad D_{12} = n_1 \frac{k}{\eta_0} \left(\Pi_2 + \sigma \pi_2 \right), \qquad (3.11a,b)$$

$$D_{21} = \ell \frac{n_2}{n_1} D_{11} - \gamma D_t, \qquad D_{22} = \ell \frac{n_2}{n_1} D_{12} + D_t, \qquad (3.11c,d)$$

where $\ell = (\sigma + \alpha - 1)/\alpha$ is a cross-diffusion factor and $\gamma = -\pi_1/\pi_2$ is a preferential interaction coefficient. Equations (3.11) are written in terms of the experimental quantities $\{\Pi, \pi, k, \sigma, \alpha, D_t\}$, which replace the phenomenological coefficients and chemical potentials in (2.5). In Section 4, theoretical and semi-empirical expressions for these quantities are obtained as functions of the host-particle volume fraction ϕ_1.

4. Volume fraction dependence

4.1. *Host matrix permeability*

In the tracer limit ($\phi_2 \to 0$), the permeability of the host particle matrix depends only on the volume fraction ϕ_1 of the host particles (Thies-Weesie & Philipse 1994). The permeability can then be written in the form

$$k = \frac{K}{6\pi R_1 n_1} = \frac{2R_1^2}{9\phi_1} K, \qquad (4.1)$$

where $K(\phi_1)$ is the dimensionless bulk mobility coefficient (sedimentation coefficient) of the host particle matrix (Russel *et al.* 1989; Peppin *et al.* 2005). Gilleland *et al.* (2011) and Fiore *et al.* (2018) suggest using a modified Richardson-Zaki equation

$$K = \frac{(1 - \phi_1)^m}{1 + (6.55 - m)\phi_1}, \qquad (4.2)$$

which agrees with Batchelor's result $K = 1 - 6.55\,\phi_1$ in the dilute limit $\phi_1 \to 0$ (Batchelor 1976). Choosing $m = 3.9$ yields a good fit to data and gives similar predictions to the Kozeny-Carman equation near close-packing (figure 2*a*). For spherical particles the Kozeny-Carman equation is $k = R_1^2 (1 - \phi_1)^3 / 45\phi_1^2$ (Carman 1939), so that (4.1) gives

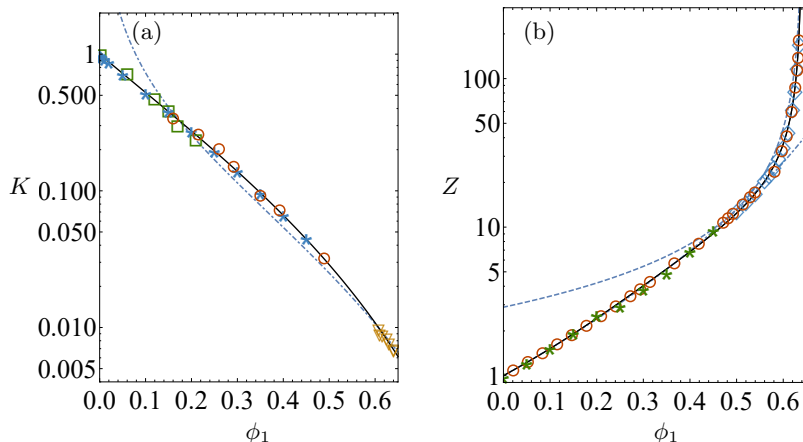$$K = \frac{(1 - \phi_1)^3}{10\phi_1} \qquad (4.3)$$

FIGURE 2. Plots of (a) the mobility function $K(\phi_1)$ and (b) the compressibility factor $Z(\phi_1)$. In (a) the data are from the sedimentation experiments of Xue *et al.* (1992) (circles) and Buzzaccaro *et al.* (2008) (squares); from the numerical simulations of (Ladd 1990) (stars); and from the permeation experiments of Carman (1939) (triangles). The curves in (a) are from equation (4.2) (solid) and from the Kozeny-Carman equation (4.3) (dash-dot). In (b) the data are from the sedimentation experiments of Buzzaccaro *et al.* (2007) (stars) and the molecular dynamics simulations of Wu & Sadus (2005) (circles) and Rintoul & Torquato (1996) (diamonds). The curves are from equation (4.6) (solid), from the Carnahan-Starling equation of state (4.5) (dash-dot) and the Woodcock equation of state (dash).

as the Kozeny-Carman sedimentation coefficient (Philipse & Pathmamanoharan 1993). Equation (4.3) is plotted on figure 2*a* as the dash-dot curve.

4.2. *Osmotic pressures*

4.2.1. *Host particles*

Similarly to k, in the dilute tracer limit $\phi_2 \to 0$, the host osmotic pressure Π depends only on ϕ_1 (Lekkerkerker & Stroobants 1993). The osmotic pressure can then be written as

$$\Pi = n_1 k_B T Z, \tag{4.4}$$

where $Z(\phi_1)$ is the hard-sphere compressibility factor (Russel *et al.* 1989). Over the range $(0 < \phi_1 < 0.55)$, Z is given approximately by the Carnahan-Starling equation

$$Z = \frac{1 + \phi_1 + \phi_1^2 - \phi_1^3}{(1 - \phi_1)^3} \tag{4.5}$$

(Carnahan & Starling 1969), while at higher volume fractions Z diverges according to Woodcock's equation $Z \sim (1 - \phi_1/\phi_p)^{-1}$, where $\phi_p = 0.64$ is the volume fraction at random close packing (Woodcock 1981; Russel *et al.* 1989; O'Hern *et al.* 2003). The following combined expression,

$$Z(\phi_1) = \frac{1 + 2.45\phi_1 + 2.2\phi_1^2 + 20\phi_1^3 - 41\phi_1^4}{1 - \phi_1/\phi_p}, \tag{4.6}$$

agrees with the Carnahan-Starling equation as $\phi_1 \to 0$ and with the Woodcock equation as $\phi_1 \to \phi_p$. Equation (4.6) is plotted on figure 2*b* along with data from sedimentation experiments (Buzzaccaro *et al.* 2007) and molecular dynamics simulations (Rintoul &

Torquato 1996; Wu & Sadus 2005). The first two coefficients in the numerator of equation (4.6) were determined by requiring that $Z \to 1 + 4\phi_1$ as $\phi_1 \to 0$ (Carnahan & Starling 1969); the remaining three coefficients were treated as adjustable parameters to achieve a best fit to the data. While more exact and complex equations of state have been developed (Liu 2006; Tian *et al.* 2010), equation (4.6) has a relatively simple form while maintaining accuracy near ϕ_p. Differentiating (4.4) with respect to n_i gives

$$\Pi_1 = k_B T \frac{\mathrm{d}(\phi_1 Z)}{\mathrm{d}\phi_1} \quad \text{and} \quad \Pi_2 = 0. \tag{4.7}$$

4.2.2. *Tracer particles*

Assuming the tracer concentration in the reservoir compartment B is dilute the osmotic pressure π is

$$\pi = n_2^r k_B T. \tag{4.8}$$

Differentiating π with respect to n_i gives, bearing in mind that $n_2^r = n_2/\alpha$ and assuming $\alpha = \alpha(n_1)$ (Lekkerkerker & Stroobants 1993),

$$\pi_1 = -\frac{n_2 \alpha_1 \pi_r}{\alpha^2} \quad \text{and} \quad \pi_2 = \frac{\pi_r}{\alpha}, \tag{4.9}$$

where $\alpha_1 = (\partial \alpha / \partial n_1)_{T,P,n_2}$ and $\pi_r = (\partial \pi / \partial n_2^r)_{T,p} = k_B T$.

4.3. *Equilibrium partition coefficient*

The partition coefficient α can be obtained by equating the chemical potential of the tracer particles in the suspension and reservoir of figure 1. In the dilute limit ($\phi_2 \ll \phi_1 \ll 1$), equation (2.7b) gives the chemical potential of the tracer particles in the suspension (compartment A) as

$$\mu_2 = \mu_2^0 + k_B T(\ln\phi_2 + b_{12}\phi_1). \tag{4.10}$$

When $\phi_2^r \ll 1$ the chemical potential of the tracer particles in the reservoir is

$$\mu_r = \mu_2^0 + k_B T \ln\phi_2^r, \tag{4.11}$$

where $\phi_2^r = v_2 n_2^r$ is the tracer volume fraction in the reservoir. Equating the chemical potentials at equilibrium, $\mu_2 = \mu_2^r$, gives the partition coefficient as

$$\alpha = \frac{\phi_2}{\phi_2^r} = \mathrm{e}^{-b_{12}\phi_1}. \tag{4.12}$$

As $\phi_1 \to 0$, (4.12) becomes

$$\alpha = 1 - b_{12}\phi_1 = 1 - v_{ex}n_1, \tag{4.13}$$

where $v_{ex} = b_{12}v_1 = \frac{4}{3}\pi(R_1 + R_2)^3$ is the volume excluded to the center of a tracer particle by a host particle. Thus in the dilute limit α is a measure of the free volume fraction available to the tracer particles (Lekkerkerker & Stroobants 1993; Annunziata 2008). When $R_2 \ll R_1$, α is equal to the void fraction $1 - \phi_1$.

4.4. *Preferential interaction coefficient*

The preferential interaction coefficient appearing in equation (3.11c) is

$$\gamma = -\frac{\mu_{21}}{\mu_{22}} = -\frac{\pi_1}{\pi_2} = \left(\frac{\partial n_2}{\partial n_1}\right)_{T,P,\pi}, \tag{4.14}$$

and measures the number of tracer particles that must be added to compartment A of figure 1 per added host particle, in order to maintain $\pi(n_2^r)$ constant in compartment

B. For charged proteins and adsorbing colloids, γ can be positive or negative (Schneider & Trout 2009); however, for hard-sphere systems involving only volume exclusion γ is negative (the host particles exclude tracer particles). With equations (4.9) and (4.12) the preferential interaction coefficient γ is

$$\gamma = n_2 \frac{\alpha_1}{\alpha} = -n_2 v_1 b_{12} = -n_2 v_{ex}. \tag{4.15}$$

Thus, for each additional host particle added to compartment A of figure 1, $n_2 v_{ex}$ tracer particles must be removed in the dilute limit to maintain osmotic equilibrium with compartment B.

4.5. *Tortuosity and reflection coefficient*

4.5.1. *Definition and dilute limit*

The diffusive tortuosity factor τ is defined as the ratio of the tracer diffusivity D_t in the suspension to the Stokes-Einstein diffusivity $D_2^0 = k_B T / 6\pi R_2 \eta_0$ of a tracer particle in the pure suspending fluid:

$$\tau \equiv D_t / D_2^0. \tag{4.16}$$

In the dilute limit an expression for τ can be obtained using Batchelor's equations (2.6). Equation (3.10c) combined with (2.6) and (4.8) gives in the limit $\phi_2 \ll \phi_1 \ll 1$ as

$$\tau = 1 - \tau_1 \phi_1, \tag{4.17}$$

where $\tau_1 = -K'_{21} = 2.5\lambda_{12}/(\lambda_{12} + .22)$. Similarly, equation (3.10b) can be combined with (4.13) and (2.6a,b) in the limit $\phi_2 \ll \phi_1 \ll 1$ to obtain

$$\sigma = \sigma_1 \phi_1, \tag{4.18}$$

where $\sigma_1 = b_{12} + K''_{12}$. Equation (4.18) shows that, because of excluded volume and long-range viscous effects, the host particles have a 'membrane separation' effect ($\sigma > 0$) on the tracer particles even in the dilute limit. Only when the tracer particles have negligible volume ($\lambda_{12} = R_2/R_1 \to 0$) does σ reduce to zero. In concentrated suspensions, $\tau(\phi_1)$ and $\sigma(\phi_1)$ can be obtained using results of hindered diffusion models of tracer particles in cylindrical pores, as detailed below.

4.5.2. *Cylindrical pores*

Expressions for τ and σ of spherical tracer particles in cylindrical pores have been derived by Anderson & Quinn (1974) in the form

$$\tau = (1 - \lambda)^2 K_d, \tag{4.19}$$

and

$$\sigma = 1 - (1 - \lambda)^2 K_c, \tag{4.20}$$

where $K_c(\lambda)$ and $K_d(\lambda)$ are hydrodynamic factors and $\lambda = R_2/R_p$ is the ratio of tracer particle radius R_2 to the pore radius R_p. Equations (4.20) and (4.19) assume the tracer particles are equal to or smaller than the pore radius ($\lambda \leqslant 1$). When $\lambda > 1$, $\sigma = 1$ and $\tau = 0$ since the tracer particles in this case cannot enter the pores.

For $\lambda \leqslant 0.4$, Anderson & Quinn (1974) obtained $K_c = (1 + 2\lambda - \lambda^2)(1 - \frac{2}{3}\lambda^2 - 0.163\lambda^3)$ and $K_d = 1 - 2.1\lambda + 2.09\lambda^3 - 0.95\lambda^5$. Recent finite element simulations (Oatley-Radcliffe *et al.* 2015), valid over the range $0 \leqslant \lambda \leqslant .98$, can be fit by the empirical equations

$$K_c = (1 + 2\lambda - \lambda^2)(1 - 0.81\lambda^2 + 0.31\lambda^3) \tag{4.21}$$
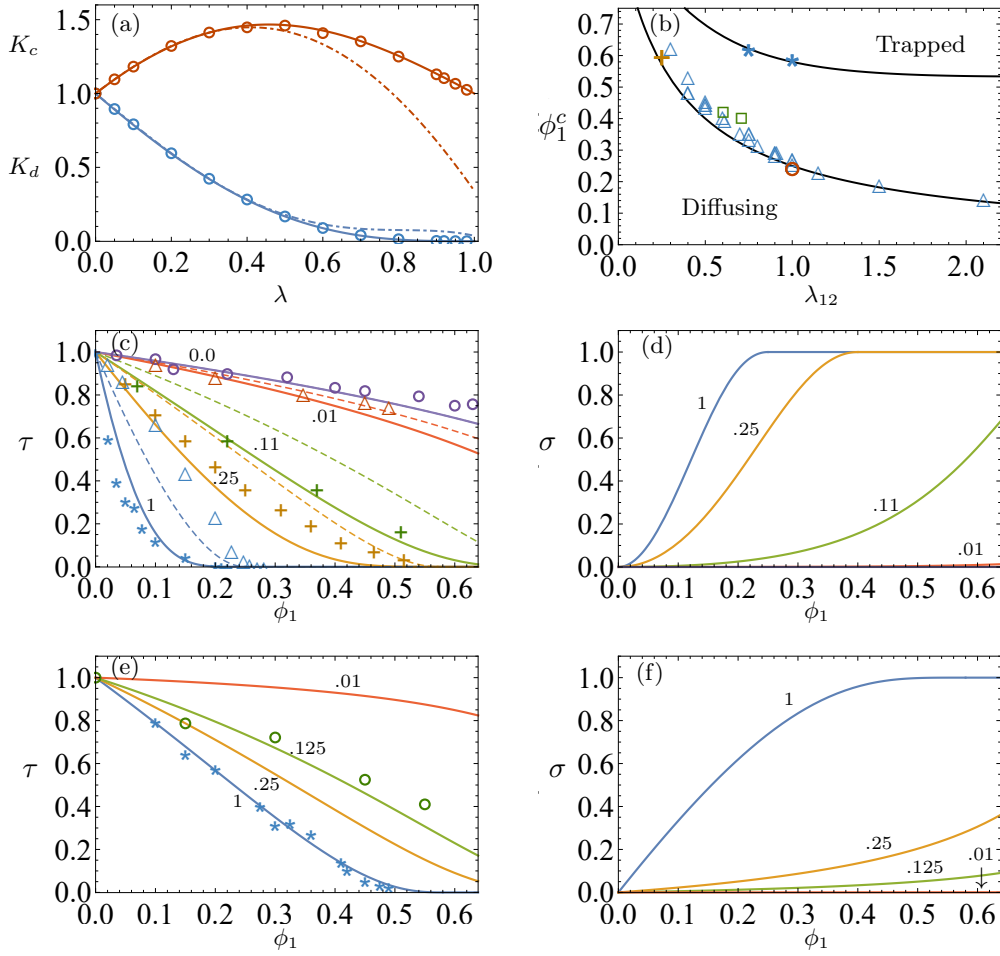
FIGURE 3. (a) Convective and diffusive hydrodynamic factors K_c (top) and K_d (bottom), respectively, plotted versus the tracer/cylindrical-pore size ratio $\lambda = R_2/R_p$. The circles are data from finite element simulations (Oatley-Radcliffe *et al.* 2015); the dash-dot curves are from the theory of Anderson & Quinn (1974) (valid for $\lambda \leqslant 0.4$); and the solid curves are from equations (4.21) and (4.22). (b) Trapping volume fraction $\phi_1^c(\lambda_{12})$ for tracer diffusion in porous media (lower curve) and suspensions (upper curve), plotted versus the tracer/host particle size ratio $\lambda_{12} = R_2/R_1$. The data are from Kim & Torquato (1992) (cross), Gimel & Taco (2011) (triangles), Sung & Yethiraj (2008) (circle), Lockett & Al-Habbooby (1974) (squares) and Zaccarelli *et al.* (2015) (stars). (c) Porous media tortuosity factor $\tau(\phi_1)$ calculated from equation (4.25) for different values of λ_{12}. The dashed curves are from (4.25) with $K_d = 1$. The data are from Neale & Nader (1973) (circles), Kim & Torquato (1992) (crosses) Sung & Yethiraj (2008) (stars) and Gimel & Taco (2011) (triangles). (d) Porous media reflection coefficient $\sigma(\phi_1)$ for the same size ratios as in figure (c), calculated from equation (4.26). (e) Suspension tortuosity factor $\tau(\phi_1)$ calculated from equation (4.28) for several values of λ_{12}, with data from Segrè *et al.* (1995) (stars) and Guan *et al.* (2014) (circles). (f) Suspension reflection coefficient $\sigma(\phi_1)$ for the same size ratios as in figure (e), calculated from equation (4.29). The numbers next to the curves in (c-f) are the values of λ_{12}.

and

$$K_d = (1 - \lambda)^{2.2+0.55\lambda}, \tag{4.22}$$

as shown on figure 3a.

4.5.3. *Porous media*

Equations (4.20)–(4.22) can be applied to porous media by noting that the approximate physical pore radius is $R_p = \epsilon/S_p(1-\epsilon)$, where $\epsilon = 1 - \phi_1$ is the void fraction and S_p is the specific surface area of the porous matrix (Carman 1939). For a matrix composed of sherical particles $S_p = 4\pi R_1^2/\frac{4}{3}\pi R_1^3 = 3/R_1$ (Bird *et al.* 2002), giving

$$\lambda_p = \frac{R_2}{R_p} = \frac{3\lambda_{12}\phi_1}{(1-\phi_1)}. \tag{4.23}$$

In porous media there is in addition a geometric tortuosity τ_g related to the increased length of the meandering pathways tracer particles take through the pore space relative to straight cylindrical pores (Malusis *et al.* 2012; Ghanbarian *et al.* 2013). For spherical matrix particles Delgado (2006) obtains

$$\tau_g = (1 - \phi_1)^{0.4}. \tag{4.24}$$

The tortuosity and reflection coefficient can then be written as

$$\tau = \begin{cases} \tau_g(1-\lambda_p)^2 K_d(\lambda_p) & \text{if } 0 \leqslant \lambda_p \leqslant 1 \\ 1 & \text{if } \lambda_p > 1 \end{cases} \tag{4.25}$$

and

$$\sigma = \begin{cases} 1 - (1-\lambda_p)^2 K_c(\lambda_p) & \text{if } 0 \leqslant \lambda_p \leqslant 1 \\ 1 & \text{if } \lambda_p > 1. \end{cases} \tag{4.26}$$

Figures 3c and d show τ and σ plotted versus ϕ_1 for several values of λ_{12}, along with experimental data for τ from Neale & Nader (1973) and numerical data from Kim & Torquato (1992), Sung & Yethiraj (2008) and Gimel & Taco (2011). As the numerical simulations did not include viscous effects, also shown on figure 3c are results from (4.25) with the hydrodynamic factor K_d set to 1 (dashed curves).

In the dilute host limit ($\phi_1 \ll 1$), the pore size is large ($R_p \gg R_2$) and the host particles have little effect on the tracer diffusion, so that $\tau \to 1$ and $\sigma \to 0$. At higher matrix concentrations the pore radius R_p approaches the tracer radius R_2 and the tracer diffusion is strongly hindered ($\tau < 1$). At a critical host volume fraction ϕ_1^c, $R_p = R_2$ and the particles are trapped within the pores, so that $\tau = 0$ and $\sigma = 1$. Setting $\lambda_p = 1$ in equation (4.23) gives

$$\phi_1^c = (1 + 3\lambda_{12})^{-1}, \tag{4.27}$$

so that $\phi_1^c = 0.25$ when $\lambda_{12} = 1$. Figure 3b (lower curve) shows ϕ_1^c plotted versus λ_{12} along with experimental and numerical data from Kim & Torquato (1992), Sung & Yethiraj (2008) and Gimel & Taco (2011). In the case of small tracer particles ($\lambda_{12} \leqslant .11$ in figure 3c) the particles are hindered by the host matrix as ϕ_1 increases, but can still diffuse throughout the pore space even up to the close-packed limit $\phi_p = 0.64$.

4.5.4. *Suspensions*

In contrast to porous media where the matrix is fixed in place, in suspensions the host particles are able to move in response to viscous and Brownian forces (Wang & Brady 2015; Bruna & Chapman 2015; Sentjabrskaja1 *et al.* 2016). Tracer particles in suspensions therefore can diffuse even when the tracer radius R_2 is larger than the pore size R_p; the host particles can adjust their positions, opening dynamic heterogeneities through which the tracer particles can pass (Rallison 1988; Kumar *et al.* 2006; Wang *et al.* 2012; Guan *et al.* 2014). Previously, this effect has been modelled phenomenologically by assuming the host suspension is composed of fast and slow domains having different viscosities

(Hodgdon & Stillinger 1993; Xia & Wolynes 2001; Fan *et al.* 2007) or by introducing a scaling factor for the tracer radius (Kalwarczyk *et al.* 2014). A similar method used here is to assume the tracer particles in suspensions experience an effective *diffusive* pore size $R_d = c_d R_p$, where $c_d > 1$ is an empirical scaling factor to be determined. Assuming power laws for τ and σ of the form

$$\tau = \begin{cases} (1 - \lambda_d)^{a_\tau} & \text{if } 0 \leqslant \lambda_d \leqslant 1 \\ 1 & \text{if } \lambda_d > 1 \end{cases} \tag{4.28}$$

and

$$\sigma = \begin{cases} 1 - (1 - \lambda_d)^{a_\sigma} & \text{if } 0 \leqslant \lambda_d \leqslant 1 \\ 1 & \text{if } \lambda_d > 1 \end{cases} \tag{4.29}$$

where

$$\lambda_d = \frac{3\lambda_{12}\phi_1}{c_d(1 - \phi_1)}, \tag{4.30}$$

the exponents a_τ and a_σ can be obtained by requiring (4.28) and (4.29) to match (4.17) and (4.18) in the limit $\phi_1 \to 0$. In this limit (4.28) and (4.29) become $\tau = 1 - 3\lambda_{12}a_\tau\phi_1/c_d$ and $\sigma = 3\lambda_{12}a_\sigma\phi_1/c_d$ giving

$$a_\tau = \frac{\tau_1 c_d}{3\lambda_{12}} \quad \text{and} \quad a_\sigma = \frac{\sigma_1 c_d}{3\lambda_{12}}. \tag{4.31}$$

A fit of (4.28) to data for the viscosity of a hard-sphere suspension (Section 6.1) gives

$$c_d = 3\frac{\phi_g}{(1 - \phi_g)}\frac{(1 + \lambda_{12}^2)}{(1 + \lambda_{12})}, \tag{4.32}$$

where $\phi_g = 0.58$ is the volume fraction at the hard-sphere glass transition (Hunter & Weeks 2012).

The tortuosity $\tau(\phi_1)$ and reflection coefficient $\sigma(\phi_1)$ calculated from equations (4.28)–(4.32) are plotted on figure 3*e,f* for several values of the particle size ratio $\lambda_{12} = R_2/R_1$, along with experimental data from Segrè *et al.* (1995) and Guan *et al.* (2014). The critical trapping volume fraction ϕ_1^c at which $\tau = 0$ in suspensions can be obtained by setting $\lambda_d = 1$ in (4.30) giving

$$\phi_1^c = (1 + 3\lambda_{12}/c_d)^{-1}. \tag{4.33}$$

Equation (4.33) is plotted as the upper curve in figure 3*b*, along with estimates of ϕ_1^c from the data of Zaccarelli *et al.* (2015). In suspensions the tracer diffusion is significantly less hindered than in porous media – in the self-diffusion case $\lambda_{12} = 1$, tracer diffusion ceases at the glass transition $\phi_1^c = 0.58$, while for porous media $\phi_1^c = 0.25$.

4.6. *Cross-diffusion factor*

The cross-diffusion factor in (3.11*c*) is

$$\ell = \left(\frac{\sigma + \alpha - 1}{\alpha}\right) = \frac{n_1}{n_2}\frac{L_{12}}{L_{11}}, \tag{4.34}$$

and is a measure of fluid-mediated friction interactions between the tracer and host particles. In the dilute limit ($\phi_2 \ll \phi_1 \ll 1$), equations (4.13) and (4.18) give

$$\ell = K_{12}^{''}\phi_1. \tag{4.35}$$

At higher host volume fractions ℓ can be obtained using (4.34) with (4.29) for $\sigma(\phi_1)$ and (4.12) for $\alpha(\phi_1)$. At host volume fractions above ϕ_1^c where $\sigma = 1$, equation (4.34) gives $\ell = 1$.
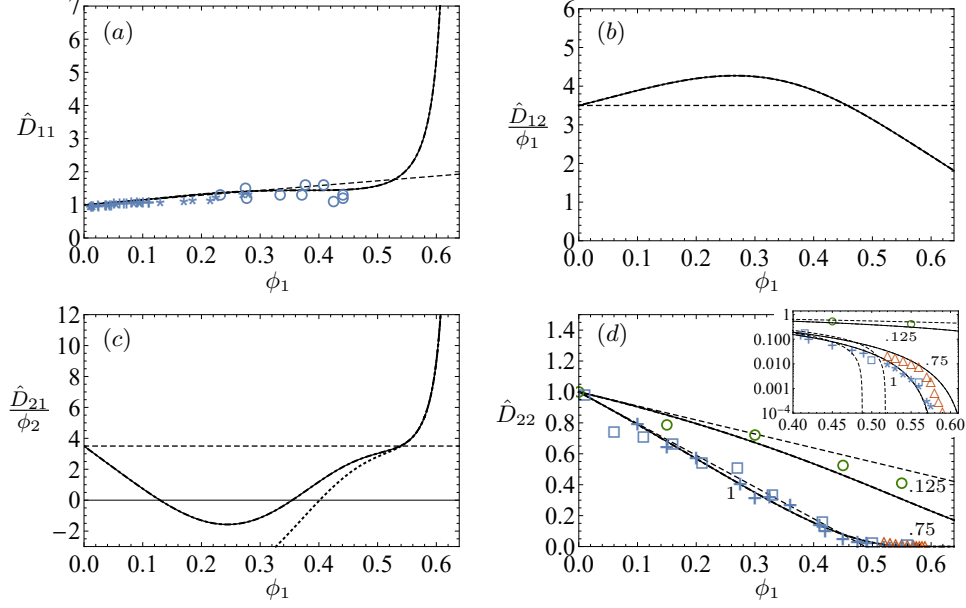
Figure 4. Plots of the dimensionless diffusion and cross-diffusion coefficients calculated from equations (5.1) as functions of ϕ_1 for $\phi_2 = 10^{-5}$ and $\lambda_{12} = 1$: (a) host particle Fickian diffusion coefficient $\hat{D}_{11}$; (b) host particle cross-diffusion coefficient $\hat{D}_{12}$; (c) tracer cross-diffusion coeffient $\hat{D}_{21}$; (d) tracer Fickian diffusion coefficient $\hat{D}_{22}$. The host and tracer cross-diffusion coefficients have been scaled with the volume fractions ϕ_1 and ϕ_2. The solid curves are from equations (5.1); the dash-dot curves (nearly indistinguishable) are from the approximate equations (5.2). The dashed lines are from Batchelor's equations (2.9). The dotted curve in figure (c) is from equation (5.3). The experimental data in (a) are from Kops-Werkhoven & Fijnaut (1981) (crosses), van Megen et al. (1985) (circles) and De Kruif & Vrij (1987) (stars); the data in (d) are from Segrè et al. (1995) (crosses), Pryamitsyn & Ganesan (2005) (squares) and Zaccarelli et al. (2015) (stars) for $\lambda_{12} = 1$; from Zaccarelli et al. (2015) (diamonds) for $\lambda_{12} = .75$; and from Guan et al. (2014) (circles) for $\lambda_{12} = .125$. The inset shows the high-concentration $\hat{D}_{22}(\phi_1)$ data and results on a log scale.

5. Diffusion and cross-diffusion coefficients

With the results of Section 4, equations (3.11) can be used to calculate the diffusion coefficients D_{ij} as functions of ϕ_1. In terms of dimensionless quantities equations (3.11) can be written as

$$\hat{D}_{11} = K(\hat{\Pi}_1 + \sigma \hat{\pi}_1), \qquad \hat{D}_{12} = K(\hat{\Pi}_2 + \sigma \hat{\pi}_2), \qquad (5.1a,b)$$

$$\hat{D}_{21} = \hat{\ell} \hat{D}_{11} - \gamma\tau, \qquad \hat{D}_{22} = \hat{\ell} \hat{D}_{12} + \tau, \qquad (5.1c,d)$$

where $\hat{D}_{ij} = D_{ij}/D_i^0$, $\hat{\Pi}_i = \Pi_i/k_B T$, $\hat{\pi}_i = \pi_i/k_B T$ and $\hat{\ell} = \phi_2 \ell / \phi_1 \lambda_{12}^2$. The $\hat{D}_{ij}$ are plotted on figure 4 as functions of ϕ_1 for the case $\phi_2 = 10^{-5}$ and $\lambda_{12} = 1$, along with experimental data and Batchelor's equations (2.9) (dashed lines). When the tracer particles are sufficiently dilute that $\phi_2 \ll \alpha$ (corresponding via equation (4.12) to $\phi_2^r \ll 1$), then several terms involving ϕ_2 in (3.11) can be neglected, yielding the simpler equations

$$\hat{D}_{11} = K\hat{\Pi}_1, \qquad \hat{D}_{12} = K\sigma\hat{\pi}_2, \qquad (5.2a,b)$$

$$\hat{D}_{21} = \hat{\ell} \hat{D}_{11} - \gamma\tau, \qquad \hat{D}_{22} = \tau, \qquad (5.2c,d)$$

Equations (5.2) are plotted on figure 4 as the dash-dot curves; for the case $\phi_2 = 10^{-5}$ they are nearly indistinguishable from the solid curves. If in addition $\tau \ll 1$ (crowded

host matrix), then the $\gamma\tau$ term in (5.2c) can also be neglected, so that

$$\hat{D}_{21} = \hat{\ell}\hat{D}_{11}. \tag{5.3}$$

Equation (5.3) is plotted on figure 4c as the dotted curve, which agrees with (5.2c) when $\phi_1 \gtrsim 0.5$.

The behaviour of $\hat{D}_{11}$ (figure 4a) is similar to that observed in previous works on diffusion in hard-sphere suspensions (Auzerais *et al.* 1988; Peppin *et al.* 2006). The slope of the diffusivity curve is reduced, relative to the dilute case, at intermediate ϕ_1 because of viscous drag, but eventually diverges as $\phi_1 \to \phi_p$ owing to the infinite repulsion between hard-sphere particles at contact (Auzerais *et al.* 1988). The host particle cross-diffusion coefficient $\hat{D}_{12}$, being proportional to σ, increases with ϕ_1 (figure 4b); viscous drag, accounted for by the mobility $K(\phi_1)$, works to reduce the value of $\hat{D}_{12}$ as ϕ_1 approaches ϕ_p. The tracer cross diffusion coefficient $\hat{D}_{21}$ (figure 4c) is predicted to at first decrease with ϕ_1, even dipping below 0, owing to the cross-diffusion factor ℓ, which is negative at low ϕ_1 (equation (4.35)). While negative cross-diffusion coefficients have been observed experimentally (Annunziata *et al.* 2000), the results for $\hat{D}_{21}$ must be viewed with caution as they depend strongly on $\sigma(\phi_1)$, and without experimental data it is difficult to make firm conclusions. $\hat{D}_{21}$ is predicted to diverge as $\phi_1 \to \phi_p$, owing to the fact that $\ell \to 1$ and $\hat{D}_{11} \to \infty$ as $\phi_1 \to \phi_p$. The main Fickian tracer diffusivity $\hat{D}_{22}$ approaches zero in this limit (figure 4d), suggesting that the transport of tracer particles at concentrations near to and above the glass transition could be strongly affected by cross diffusion. The tracer diffusivity $\hat{D}_{22}(\phi_1)$ (figure 4d) decreases with ϕ_1 because of the reduced pore space available for diffusion. For $\lambda_{12} = 1$, $\hat{D}_{22}$ approaches zero at the glass transition $\phi_1 = \phi_g$, while for $\lambda_{12} = 0.125$ $\hat{D}_{22}$ remains above zero at all volume fractions including the close packing limit $\phi_1 = \phi_p$.

Batchelor's equations (2.9) are in good agreement with the data for $\hat{D}_{11}$ and $\hat{D}_{22}$, well beyond the dilute limit up to $\phi_1 \approx 0.45$. As ϕ_1 approaches the glass transition $\phi_g = 0.58$ the data for $\hat{D}_{22}$ departs from Batchelor's solution and agrees more closely with (5.1d), as shown in the inset to figure 4d. Unfortunately, no data is available for $\hat{D}_{11}$ near the glass transition, nor is any data available for the cross-diffusion coefficients in hard-sphere suspensions with which to compare equations (5.1b,c). Data for all four diffusion coefficients have been obtained for a range of polymer and protein solutions (Vergara *et al.* 2004; Annunziata *et al.* 2009). It is possible the results obtained here could be adapted to such systems by using an *effective* hard sphere model (Minton 2007), though this is beyond the scope of the present work.

6. Discussion

The development in Section 4 contains several approximations leading to the expressions for σ, τ and for the D_{ij}. While agreement with experiment for D_{11} and D_{22} is good, the results for D_{12} and D_{21} are less certain and there is a need for experimental data. Nevertheless, the expressions (3.11) for the D_{ij} should hold quite generally, and the development in Section 4 can be updated as new data and theories become available. In this section the results are applied to study the breakdown of the Stokes-Einstein equation near the glass transition, to sedimentation in binary suspensions, and to the physical interpretation and measurement of the reflection coefficient σ.
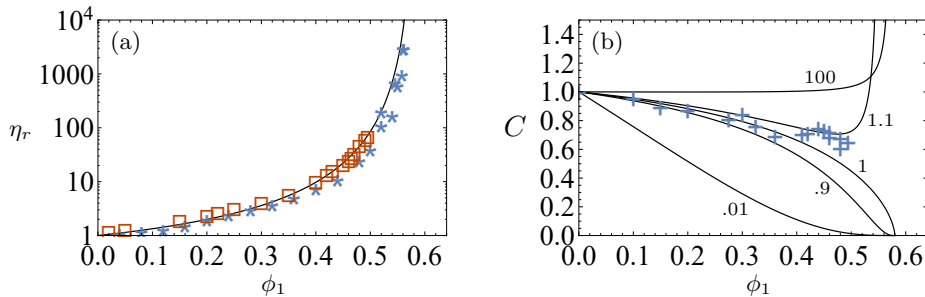
FIGURE 5. (a) Relative low-shear viscosity $\eta_r = \eta/\eta_0$ of a hard-sphere suspension. The curve is from equation (6.2); the data are from (Segrè *et al.* 1995) (squares) and Russel *et al.* (2013) (stars). (b) Parameter C quantifying the breakdown of the Stokes-Einstein equation (6.1). When $C = 1$ the Stokes-Einstein equation holds, while larger/smaller values of C imply reduced/enhanced diffusion of the tracer particles. The solid curves are from equation (6.4); the numbers next to the curves are the values of λ_{12}. The data are from (Segrè *et al.* 1995) for the self-diffusion case $\lambda_{12} = 1$.

6.1. *Viscosity and the Stokes-Einstein equation*

When $R_2 \gg R_1$ (very large tracer particles) the host suspension behaves like an effective continuum within which the tracer particles diffuse. The diffusivity of a tracer particle is then given by the Stokes-Einstein equation

$$D_t = D_{SE} = \frac{k_B T}{6\pi R_2 \eta}, \tag{6.1}$$

where $\eta(\phi_1)$ is the viscosity of the host particle suspension (Sutherland 1905; Einstein 1956; Kalwarczyk *et al.* 2014). Equations (6.1), (4.16), (4.28) and (4.30)–(4.32) can be combined in the limit $\lambda_{12} \to \infty$ to give

$$\eta = \lim_{\lambda_{12} \to \infty} \frac{\eta_0}{\tau} = \eta_0 \left(1 - \frac{\phi_1(1-\phi_g)}{\phi_g(1-\phi_1)} \right)^{-2.5\frac{\phi_g}{1-\phi_g}}. \tag{6.2}$$

Equation (6.2) is similar to an equation for η derived by Faroughi & Huber (2015), and is plotted on figure 5a along with experimental data from Segrè *et al.* (1995) and Russel *et al.* (2013). The fit is quite good, supporting equation (4.32) for the scaling factor c_d.

In studies of the breakdown of the Stokes-Einstein relation the tracer diffusivity is often written in the form

$$D_t = \frac{k_B T}{C 6\pi R_2 \eta}, \tag{6.3}$$

where $C = D_{SE}/D_t$ is a factor such that when $C \neq 1$ there is a deviation of the tracer diffusivity from the Stokes-Einstein equation (6.1) (Edward 1970; Segrè *et al.* 1995; Mackowiak *et al.* 2011). Comparing with equation (4.16) gives

$$C = \frac{\eta_0}{\eta \tau}. \tag{6.4}$$

Equation (6.4), with (6.2) for η and (4.28) for τ, is plotted on figure 5b versus ϕ_1 for several values of the particle size ratio λ_{12}, along with data from Segrè *et al.* (1995) for the self-diffusion case $\lambda_{12} = 1$. The agreement is good for $\phi_1 < 0.4$, providing additional support for (4.32). In the self-diffusion case C is less than 1, implying that self-diffusion is enhanced compared to Stokes-Einstein diffusion. There is a clear breakdown of the Stokes-Einstein equation ($C \to 0$) as the glass transition is approached (Kumar *et al.* 2006; Mackowiak *et al.* 2011). Near the glass transition, however, the value of C is very

sensitive to the value of λ_{12}. For very small tracers ($\lambda_{12} \leqslant 0.01$), $\tau \approx 1$ and $C = \eta_0/\eta$ so that D_t is equal to the Stokes-Einstein diffusivity of a tracer in the pure solvent, $D_t = k_B T/6\pi R_2 \eta_0$. For large tracers ($\lambda_{12} \geqslant 100$), $C = 1$ over nearly the whole range in ϕ_1, failing only as $\phi_1 \to \phi_g$; equation (6.4) suggests that diffusion is reduced ($C > 1$) for large tracers near the glass transition (Mackowiak *et al.* 2011).

6.2. *Physical interpretation of τ and σ*

In general the tracer diffusivity can be written in the form

$$D_t = \frac{k_B T}{6\pi R_2 \eta_{\text{eff}}}, \tag{6.5}$$

where $\eta_{\text{eff}} = C\eta = \eta_0/\tau$ is an effective viscosity that depends on the tracer radius and the pore size of the host matrix (Fan *et al.* 2007; Holyst *et al.* 2009; Kalwarczyk *et al.* 2014). Physically, $\tau = \eta_0/\eta_{\text{eff}}$ represents a dimensionless viscous drag force experienced by the tracer particles within the host matrix. For $\lambda_{12} \to 0$ (vanishingly small tracer particles or infinitely large pores) the effective viscosity is equal to the pure fluid viscosity η_0 and $\tau = 1$. As R_2 increases in a given host matrix the effective viscosity η_{eff} experienced by the tracer particles also increases until, in the limit $R_2 \to \infty$, η_{eff} is equal to the macroscopic viscosity η of the host suspension (Kalwarczyk *et al.* 2014).

A physical interpretation of the colloidal reflection coefficient σ can be obtained from equation (3.11*b*), which with (4.7*b*) can be written as

$$\sigma = \frac{D_{12}}{n_1 \pi_2 k/\eta_0} = \frac{\alpha}{K}\hat{D}_{12}, \tag{6.6}$$

so that $\sigma = \hat{D}_{12}$ in the dilute limit $\phi_2 \ll \phi_1 \ll 1$. The cross-diffusion coefficient D_{12} quantifies *diffusiophoresis* – the flux of host particles induced by a gradient in tracer concentration (Anderson 1989; Annunziata *et al.* 2012). Therefore, σ is a measure of the diffusiophoretic force exerted on the host matrix by the tracer particles in the pore space. Furthermore, combining equations (3.7*a*) and (3.9*b*) shows that

$$\sigma = -\left(\frac{\boldsymbol{\nabla}\Pi}{\boldsymbol{\nabla}\pi}\right)_{q=0}. \tag{6.7}$$

Given a tracer osmotic pressure gradient $\boldsymbol{\nabla}\pi$ in compartment B of figure 6, when $\sigma = 0$ the tracer particles exert no force on the host matrix and $\boldsymbol{\nabla}\Pi = 0$. Conversely, when $\sigma = 1$ the entire tracer thermodynamic force $\boldsymbol{\nabla}\pi$ is transferred via diffusiophoresis to the host matrix, generating an equal and opposite force $\boldsymbol{\nabla}\Pi$.

6.3. *Experimental measurement of σ*

The reflection coefficient $\sigma(\phi_1)$ can in principle be measured using the setup illustrated in figure 6, which is similar to that studied numerically by Ariza & Puertas (2009) and used by Smit *et al.* (1975) for porous media. Two reservoirs, A and C, having different pressures and tracer concentrations, are placed in contact with the suspension in B across semi-permeable partitions. The tracer concentration difference Δn_2^r between the reservoirs leads to a diffusive flux J. The pressure difference Δp between the reservoirs is adjusted to ensure no volume flow ($q = 0$). For sufficiently small Δn_2^r, at steady state, σ is then determined from equation (3.9) as $\sigma = \Delta p/\Delta\pi = \Delta p/\Delta n_2^r k_B T$. Repeating the experiment for different initial values of ϕ_1 yields the function $\sigma(\phi_1)$.

An alternative method to obtain σ is to measure D_{12} via diffusiophoresis experiments (Annunziata *et al.* 2012; Anderson 1989) and use equation (6.6). It may also be possible
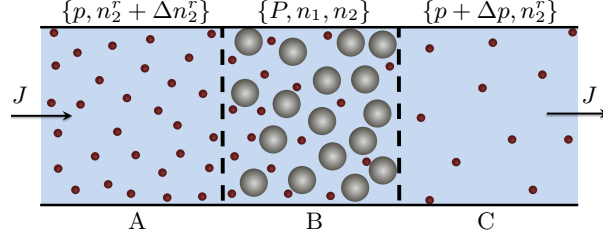
FIGURE 6. Illustration of a system for measuring the reflection coefficient σ of a colloidal suspension. The central compartment B contains a bidisperse suspension at pressure P and average host matrix volume fraction $\phi_1 = n_1 v_1$. The partition on either side of the central compartment is permeable to the fluid and tracer particles, but impermeable to the host particles. A tracer particle concentration difference Δn_2^r is maintained between compartments A and C, causing a tracer diffusive flux J. A pressure difference Δp between compartments A and C is adjusted to ensure that the volume flux q is zero. Measurements of Δn_2^r and Δp then yield σ via equation (3.9).

to obtain $\sigma(\phi_1)$ from tracer sedimentation experiments. As shown by Batchelor (1986), the particle fluxes in the homogeneous region of a sedimentation column are

$$n_1 \boldsymbol{u}_1 = L_{11} \boldsymbol{F}_1 + L_{12} \boldsymbol{F}_2, \qquad (6.8a)$$

$$n_2 \boldsymbol{u}_2 = L_{21} \boldsymbol{F}_1 + L_{22} \boldsymbol{F}_2, \qquad (6.8b)$$

where $\boldsymbol{F}_i = v_i(\rho_p - \rho_f)\boldsymbol{g}$ is the buoyancy force acting on particle i, with ρ_p the particle density and ρ_f the fluid density. With equations (3.10), (4.1), (4.8) and (4.16) equations (6.8) can be written in the tracer limit $\phi_2 \to 0$ as

$$\boldsymbol{u}_1 = K \boldsymbol{u}_1^0, \qquad (6.9a)$$

$$\boldsymbol{u}_2 = \ell \boldsymbol{u}_1 + \tau \boldsymbol{u}_2^0, \qquad (6.9b)$$

where $\boldsymbol{u}_i^0 = \boldsymbol{F}_i / 6\pi R_i \eta_0$ is the Stokes velocity of particle i in the fluid. Given $\tau(\phi_1)$, measurements of $\boldsymbol{u}_i$ can therefore be used to determine the cross-diffusion factor ℓ; given $\alpha(\phi_1)$, the reflection coefficient can then be obtained from (4.34) as $\sigma = 1 - \alpha(1 - \ell)$.

It is interesting to consider the case $\phi_1 \geqslant \phi_1^c$, where $\tau = 0$, $\sigma = 1$ and the tracer particles are trapped in the pores (Section 4.5). Equation (4.34) gives $\ell = 1$ and (6.9b) becomes $\boldsymbol{u}_2 = \boldsymbol{u}_1$, so that the tracer particles are constrained to sediment at the same speed as the host particles (Kaye & Davies 1972; Lockett & Al-Habbooby 1974; Snabre et al. 2009). Figure 3b shows data for the critical trapping volume fraction at which $\boldsymbol{u}_2 = \boldsymbol{u}_1$ in the sedimentation experiments of Lockett & Al-Habbooby (1974) (squares). The data lie close to the lower curve in figure 3b, suggesting that the expressions for σ and τ developed for porous media, equations (4.25) and (4.26), may be appropriate in this case rather than the suspension equations (4.28) and (4.29). This can be explained by the Peclet number, $Pe = u_1 R_1 / D_1^0$, which was approximately 10^8 in their system (Lockett & Al-Habbooby 1974). The timescale for sedimentation of the particles was therefore much faster than the timescale for diffusive heterogeneities to appear, and the host matrix may have behaved effectively like a porous medium. It would be interesting to compare with tracer sedimentation experiments at smaller $Pe \sim 1$ to see if ϕ_1^c shifts toward the upper curve in figure 3b.

7. Conclusion

Equations for the diffusion and cross-diffusion coefficients D_{ij} of tracer particles in hard-sphere suspensions have been obtained as functions of the host particle volume fraction ϕ_1 and particle size ratio $\lambda_{12} = R_2/R_1$. By transforming the chemical potentials and phenomenological coefficients into more experimentally-convenient quantities such as the permeability k and osmotic pressure Π, expressions have been obtained for the diffusion coefficients at volume fractions up to the close-packing limit. These expressions contain the reflection coefficient σ; a brief discussion of the physical interpretation and experimental measurement of σ in suspensions has been included. Tracer Fickian diffusion, and segregation during sedimentation, cease at a critical trapping volume fraction ϕ_1^c, which depends on the effective pore size in the suspension. Cross diffusion of the tracer particles may become increasingly important relative to Fickian diffusion at volume fractions near to and above ϕ_1^c.

REFERENCES

ANDERSON, J. L. 1989 Colloid transport by interfacial forces. *Annual Review of Fluid Mechanics* **21**, 61–99.

ANDERSON, J. L. & QUINN, J. A. 1974 Restricted transport in small pores: A model for steric exclusion and hindered particle motion. *Biophysical Journal* **14**, 130–150.

ANNUNZIATA, O. 2008 On the role of solute solvation and excluded-volume interactions in coupled diffusion. *The Journal of Physical Chemistry B* **112** (38), 11968–11975.

ANNUNZIATA, O., BUZATU, D. & ALBRIGHT, J. G. 2012 Protein diffusiophoresis and salt osmotic diffusion in aqueous solutions. *The Journal of Physical Chemistry B* **116** (42), 12694–12705.

ANNUNZIATA, O., RARD, J. A., ALBRIGHT, J. G., PADUANO, L. & MILLER, D. G. 2000 Mutual diffusion coefficients and densities at 298.15 k of aqueous mixtures of nacl and na2so4 for six different solute fractions at a total molarity of 1.500 moldm-3 and of aqueous na2so4. *Journal of Chemical & Engineering Data* **45** (5), 936–945.

ANNUNZIATA, O., VERGARA, A., PADUANO, L., SARTORIO, R., MILLER, D. G. & ALBRIGHT, J. G. 2009 Quaternary diffusion coefficients in a protein-polymer-salt-water system determined by rayleigh interferometry. *The Journal of Physical Chemistry B* **113**, 13446–13453.

ARIZA, M. J. & PUERTAS, A. M. 2009 Colloidal permeability of liquid membranes consisting of hard particles by nonequilibrium simulations. *The Journal of Chemical Physics* **131** (16), 164903.

AUZERAIS, F. M., JACKSON, R. & RUSSEL, W. B. 1988 The resolution of shocks and the effects of compressible sediments in transient settling. *Journal of Fluid Mechanics* **195**, 437462.

BATCHELOR, G. K. 1976 Brownian diffusion of particles with hydrodynamic interaction. *Journal of Fluid Mechanics* **74**, 1–29.

BATCHELOR, G. K. 1983 Diffusion in a dilute polydisperse system of interacting spheres. *Journal of Fluid Mechanics* **131**, 155–175; and Corrigendum **137**, 1983, 467–469.

BATCHELOR, G. K. 1986 Note on the onsager symmetry of the kinetic coefficients for sedimentation and diffusion in a dilute bidispersion. *Journal of Fluid Mechanics* **171**, 509–517.

BIRD, R. B., STUART, W. E. & LIGHTFOOT, E. N. 2002 *Transport Phenomena Second Edition*. N.Y.: Wiley.

BRUNA, M. & CHAPMAN, S. J. 2012 Diffusion of multiple species with excluded-volume effects. *The Journal of Chemical Physics* **137**, 204116.

BRUNA, M. & CHAPMAN, S. J. 2015 Diffusion in spatially varying porous media. *SIAM Journal of Applied Mathematics* **75**, 1648–1674.

BUZZACCARO, S., RUSCONI, R. & PIAZZA, R. 2007 "sticky" hard spheres: Equation of state, phase diagram, and metastable gels. *Phys. Rev. Lett.* **99**, 098301.

Buzzaccaro, S., Tripodi, A., Rusconi, R., Vigolo, D. & Piazza, R. 2008 Kinetics of sedimentation in colloidal suspensions. *Journal of Physics: Condensed Matter* **20** (49), 494219.

Carman, P. C. 1939 Permeability of saturated sands, soils and clays. *Journal of Agricultural Science* **29**, 262–273.

Carnahan, N. F. & Starling, K. E. 1969 Equation of state for nonattracting rigid spheres. *The Journal of Chemical Physics* **51** (2), 635–636.

De Kruif, C.G., Jansen J.W. & Vrij, A. 1987 A sterically stabilized silica colloid as a model supramolecular fluid. In *Physics of Complex and Supramolecular Fluids* (ed. S. A. Safran & N. A. Clark), pp. 315–346. Wiley Interscience.

deGroot, S. R. & Mazur, P. 1962 *Non-Equilibrium Thermodynamics*. Amsterdam: North-Holland Publishing Co.

Delgado, J. M. P. Q. 2006 A simple experimental technique to measure tortuosity in packed beds. *The Canadian Journal of Chemical Engineering* **84** (6), 651–655.

Edward, J. T. 1970 Molecular volumes and the stokes-einstein equation. *Journal of Chemical Education* **47** (4), 261.

Einstein, A. 1956 *Investigations on the theory of Brownian movement*. U.S.A.: Dover.

Fan, Tai-Hsi, Dhont, Jan K. G. & Tuinier, Remco 2007 Motion of a sphere through a polymer solution. *Phys. Rev. E* **75**, 011803.

Faroughi, S. A. & Huber, C. 2015 A generalized equation for rheology of emulsions and suspensions of deformable particles subjected to simple shear at low reynolds number. *Rheol. Acta* **54**, 85–108.

Fiore, Andrew M., Wang, Gang & Swan, James W. 2018 From hindered to promoted settling in dispersions of attractive colloids: Simulation, modeling, and application to macromolecular characterization. *Phys. Rev. Fluids* **3**, 063302.

Ghanbarian, B., Hunt, A. G., Ewing, R. P. & Sahimi, M. 2013 Tortuosity in porous media: A critical review. *Soil Science Society of America Journal* **77**, 1461–1477.

Gilleland, W. T., Torquato, S. & Russel, W. B. 2011 New bounds on the sedimentation velocity for hard, charged and adhesive hard-sphere colloids. *Journal of Fluid Mechanics* **667**, 403–425.

Gimel, J.-C. & Taco, N. 2011 Self-diffusion of non-interacting hard spheres in particle gels. *J. Phys.: Condens. Matter* **23**, 234115.

Guan, J., Wang, B. & Granick, S. 2014 Even hard-sphere colloidal suspensions display fickian yet non-gaussian diffusion. *ACS Nano* **8** (4), 3331–3336.

Hannam, S. D. W., Daivis, P. J. & Bryant, G. 2017 Dramatic slowing of compositional relaxations in the approach to the glass transition for a bimodal colloidal suspension. *Phys. Rev. E* **96**, 022609.

Hodgdon, J. A. & Stillinger, F. H. 1993 Stokes-einstein violation in glass-forming liquids. *Phys. Rev. E* **48**, 207–213.

Holyst, R., Bielejewska, A., Szymaski, J., Wilk, A., Patkowski, A., Gapiski, J., ywociski, A., Kalwarczyk, T., Kalwarczyk, E., Tabaka, M., Zibacz, N. & Wieczorek, S. A. 2009 Scaling form of viscosity at all length-scales in poly(ethylene glycol) solutions studied by fluorescence correlation spectroscopy and capillary electrophoresis. *Phys. Chem. Chem. Phys.* **11**, 9025–9032.

Hunter, G. L. & Weeks, E. R. 2012 The physics of the colloidal glass transition. *Rev. Mod. Phys.* **75**, 066501.

Kalwarczyk, T., Sozanski, K., Jakiela, S., Wisniewska, A., Kalwarczyk, E., Kryszczuk, K., Hou, S. & Holyst, R. 2014 Length-scale dependent transport properties of colloidal and protein solutions for prediction of crystal nucleation rates. *Nanoscale* **6**, 10340–10346.

Kaye, B. H. & Davies, R. 1972 Experimental investigation into the settling behaviour of suspensions. *Powder Technology* **5** (2), 61–68.

Kim, I. C. & Torquato, S. 1992 Diffusion of finitesized brownian particles in porous media. *The Journal of Chemical Physics* **96** (2), 1498–1503.

Kops-Werkhoven, M. M. & Fijnaut, H. M. 1981 Dynamic light scattering and sedimentation experiments on silica dispersions at finite concentrations. *The Journal of Chemical Physics* **74**, 1618–1625.

KUMAR, S. K., SZAMEL, G. & DOUGLAS, J. F. 2006 Nature of the breakdown in the stokes-einstein relationship in a hard sphere fluid. *The Journal of Chemical Physics* **124** (21), 214501.

LADD, A. J. C. 1990 Hydrodynamic transport coefficients of random dispersions of hard spheres. *The Journal of Chemical Physics* **93**, 3484–3494.

LEKKERKERKER, H. N. W. & STROOBANTS, A. 1993 On the spinodal instability of highly asymmetric hard sphere suspensions. *Physica A* **195**, 387–397.

LIU, H. 2006 A very accurate hard sphere equation of state over the entire stable and metstable region. *eprint arXiv:cond-mat/0605392* .

LOCKETT, M. J. & AL-HABBOOBY, H. M. 1974 Relative particle velocities in two-species settling. *Powder Technology* **10**, 67–71.

MACKOWIAK, S. A., NOBLE, J. M. & KAUFMAN, L. J. 2011 Manifestations of probe presence on probe dynamics in supercooled liquids. *The Journal of Chemical Physics* **135** (21), 214503.

MALUSIS, M. A., SHACKELFORD, C. D. & MANEVAL, J. E. 2012 Critical review of coupled flux formulations for clay membranes based on nonequilibrium thermodynamics. *Journal of Contaminant Hydrology* **138**, 40–59.

VAN MEGEN, W., OTTEWILL, R.H., OWENS, S.M. & PUSEY, P. N. 1985 Measurement of the wave-vector dependent diffusion coefficient in concentrated particle dispersions. *The Journal of Chemical Physics* **82**, 508–515.

METZLER, R., JEON, J.-H., CHERSTVY, A. G. & BARKAI, E. 2014 Anomalous diffusion models and their properties: non-stationarity, non-ergodicity, and ageing at the centenary of single particle tracking. *Phys. Chem. Chem. Phys.* **16**, 24128–24164.

MINTON, A. P. 2007 The effective hard particle model provides a simple, robust, and broadly applicable description of nonideal behavior in concentrated solutions of bovine serum albumin and other nonassociating proteins. *Journal of Pharmaceutical Sciences* **96**, 3466–3469.

NEALE, G. H. & NADER, W. K. 1973 Prediction of transport processes within porous media: Diffusive flow processes within an homogeneous swarm of spherical particles. *AIChE Journal* **19** (1), 112–119.

OATLEY-RADCLIFFE, D. L., WILLIAMS, S. R., AINSCOUGH, T. J., LEE, C., JOHNSON, D. J. & WILLIAMS, P. M. 2015 Experimental determination of the hydrodynamic forces within nanofiltration membranes and evaluation of the current theoretical descriptions. *Separation and Purification Technology* **149**, 339–348.

O'HERN, C. S., SILBERT, L. E., LIU, A. J. & NAGEL, S. R. 2003 Jamming at zero temperature and zero applied stress: The epitome of disorder. *Phys. Rev. E* **68**, 011306.

PEPPIN, S. S. L., ELLIOTT, J. A. W. & WORSTER, M. G. 2005 Pressure and relative motion in colloidal suspensions. *Physics of Fluids* **17** (5), 053301.

PEPPIN, S. S. L., ELLIOTT, J. A. W. & WORSTER, M. G. 2006 Solidification of colloidal suspensions. *J. Fluid Mech.* **554**, 147–166.

PHILIPSE, A. P. & PATHMAMANOHARAN, C. 1993 Liquid permeation (and sedimentation) of dense colloidal hard-sphere packings. *Journal of Colloid and Interface Science* **159**, 96–107.

PRYAMITSYN, V. & GANESAN, V. 2005 A coarse-grained explicit solvent simulation of rheology of colloidal suspensions. *The Journal of Chemical Physics* **122** (10), 104906.

RALLISON, J. M. 1988 Brownian diffusion in concentrated suspensions of interacting particles. *Journal of Fluid Mechanics* **186**, 471–500.

RINTOUL, M. D. & TORQUATO, S. 1996 Computer simulations of dense hardsphere systems. *The Journal of Chemical Physics* **105**, 9258–9265.

RUSSEL, W. B., SEVILLE, D. A. & SCHOWALTER, W. R. 1989 *Colloidal Dispersions*. U.K.: Cambridge University Press.

RUSSEL, W. B., WAGNER, N. J. & MEWIS, J. 2013 Divergence in the low shear viscosity for brownian hard-sphere dispersions: At random close packing or the glass transition? *Journal of Rheology* **57** (6), 1555–1567.

SANTOS, A. & RORHMANN, R. D. 2013 Chemical-potential route for multicomponent fluids. *Phys. Rev. E* **87**, 052138.

SCHNEIDER, C. P. & TROUT, B. L. 2009 Investigation of cosolute-protein preferential interaction coefficients. *Journal of Physical Chemistry B* **113** (7), 2050–2058.

SEGRÈ, P. N., MEEKER, S. P., PUSEY, P. N. & POON, W. C. K. 1995 Viscosity and structural relaxation in suspensions of hard-sphere colloids. *Phys. Rev. Lett.* **75**, 958–961.

Sentjabrskaja1, T., Zaccarelli, E., Michele, C. De, Sciortino, F., Tartaglia, P., Voigtmann, T., Egelhaaf, S. U. & Laurati, M. 2016 Anomalous dynamics of intruders in a crowded environment of mobile obstacles. *Nature Communications* **7**, 11133 (1–7).

Smit, J. A. M., Eijsermans, J. C. & Staverman, A. J. 1975 Friction and partition in membranes. *The Journal of Physical Chemistry* **79** (20), 2168–2175.

Snabre, P., Pouligny, B., Metayer, C. & Nadal, F. 2009 Size segregation and particle velocity fluctuations in settling concentrated suspensions. *Rheologica Acta* **48** (8), 855–870.

Spiegler, K. S. & Kedem, O. 1966 Thermodynamics of hyperfiltration (reverse osmosis): Criteria for efficient membranes. *Desalination* **1**, 311–326.

Sung, B. J. & Yethiraj, A. 2008 The effect of matrix structure on the diffusion of fluids in porous media. *The Journal of Chemical Physics* **128** (5), 054702.

Sutherland, W. 1905 Lxxv. a dynamical theory of diffusion for non-electrolytes and the molecular mass of albumin. *The London, Edinburgh, and Dublin Philosophical Magazine and Journal of Science* **9** (54), 781–785.

Thies-Weesie, D. M. E. & Philipse, A. P. 1994 Liquid permeation of bidisperse colloidal hard-sphere packings and the kozeny-carman scaling relation. *Journal of Colloid and Interface Science* **162**, 470–480.

Tian, J., Gui, Y. & Mulero, A. 2010 New closed virial equation of state for hard-sphere fluids. *The Journal of Physical Chemistry B* **114** (42), 13399–13402.

Vergara, A., Annunziata, O., Paduano, L., Miller, D. G., Albright, J. G. & Sartorio, R. 2004 Multicomponent diffusion in crowded solutions. 2. mutual diffusion in the ternary system tetra(ethylene glycol)naclwater. *The Journal of Physical Chemistry B* **108** (8), 2764–2772.

Vergara, A., Paduano, L., Vitagliano, V. & Sartorio, R. 2001 Multicomponent diffusion in crowded solutions. 1. mutual diffusion in the ternary system poly(ethylene glycol)400naclwater. *Macromolecules* **34**, 991–1000.

Wang, B., Kuo, J., Bae, S. C. & Granick, S. 2012 When brownian diffusion is not gaussian. *Nature Materials* **11**, 481–485.

Wang, M. & Brady, J. F. 2015 Short-time transport properties of bidisperse suspensions and porous media: A stokesian dynamics study. *The Journal of Chemical Physics* **142** (9), 094901.

Woodcock, L. V. 1981 Glass transition in the hard-sphere model and kauzmann's paradox. *Annals of the New York Academy of Sciences* **371** (1), 274–298.

Wu, G.-W. & Sadus, R. J. 2005 Hard sphere compressibility factors for equation of state development. *AIChE Journal* **51**, 309–313.

Xia, X. & Wolynes, P. G. 2001 Diffusion and the mesoscopic hydrodynamics of supercooled liquids. *The Journal of Physical Chemistry B* **105** (28), 6570–6573.

Xue, J.-Z., Herbolzheimer, E., Rutgers, M. A., Russel, W. B. & Chaikin, P. M. 1992 Diffusion, dispersion, and settling of hard spheres. *Phys. Rev. Lett.* **69**, 1715–1718.

Zaccarelli, E., Liddle, S. M. & Poon, W. C. K. 2015 On polydispersity and the hard sphere glass transition. *Soft Matter* **11**, 324–330.

Zhang, H. & Nagele, G. 2002 Tracer-diffusion in binary colloidal hard-sphere suspensions. *The Journal of Chemical Physics* **117** (12), 5908–5920.